Near-wake flow simulation of a vertical axis turbine using an actuator line model

Mendoza, Victor; Bachant, Peter; Ferreira, Carlos; Goude, Anders

DOI
10.1002/we.2277

Publication date
2019

Document Version
Accepted author manuscript

Published in
Wind Energy

Citation (APA)
Mendoza, V., Bachant, P., Ferreira, C., & Goude, A. (2019). Near-wake flow simulation of a vertical axis turbine using an actuator line model. *Wind Energy*, *22*(2), 171-188. https://doi.org/10.1002/we.2277

RESEARCH ARTICLE

Near-Wake Flow Simulation of a Vertical Axis Turbine Using an Actuator Line Model

Victor Mendoza[1], Peter Bachant[2], Carlos Ferreira[3] and Anders Goude[1]

[1] Department of Engineering Sciences, Division of Electricity, Uppsala University, Uppsala 751 21, Sweden

[2] WindESCo, Inc. 265 Franklin Street Suite 1702 Boston, MA 02110 USA

[3] Delft University Wind Energy Research Institute, TUDelft, Kluyverweg 1, 2629 HS, Delft, The Netherlands

ABSTRACT

In the present work, the near-wake generated for a vertical axis wind turbine (VAWT) was simulated using an actuator line model (ALM) in order to validate and evaluate its accuracy. The sensitivity of the model to the variation of the spatial and temporal discretization was studied, and showed a bigger response to the variation in the mesh size as compared to the the temporal discretization. The large eddy simulation (LES) approach was used to predict the turbulence effects. The performance of Smagorinsky, dynamic k-equation and dynamic Lagrangian turbulence models were tested, showing very little relevant differences between them. Generally, predicted results agree well with experimental data for velocity and vorticity fields in representative sections. The presented ALM was able to characterize the main phenomena involved in the flow pattern using a relatively low computational cost without stability concerns; identified the general wake structure (qualitatively and quantitatively), and the contribution from the blade tips and motion on it. Additionally, the effects of the tower and struts were investigated with respect to the overall structure of the wake, showing no significant modification. Similarities and discrepancies between numerical and experimental results are discussed. The obtained results from the various simulations carried out here can be used as a practical reference guideline for choosing parameters in VAWTs simulations using the ALM.

KEYWORDS

Near Wake Simulation; Vertical Axis Wind Turbine; VAWT; Actuator Line Model; Dynamic Stall Model

Correspondence

V. Mendoza, Department of Engineering Sciences, Division of Electricity, Uppsala University, Uppsala 751 21, Sweden

E-mail: victor.mendoza@angstrom.uu.se

Received . . .

1. INTRODUCTION

The current trend of the wind energy industry aims for large scale turbines in offshore farms [1–3] bringing a renewed interest in VAWTs, since they have several advantages over the conventional HAWTs, and their implementation can potentially mitigate the new challenges that the offshore environment presents [4–6]. The omni-directionality of VAWTs allow them to work with winds from any direction, resulting in a simpler mechanical design with fewer moving parts, which excludes the yawing, and often the pitching system. This is a relevant advantage since a significant amount of failures encountered in HAWTs occur in their yawing mechanism [7–9], and it is highly appreciated in an offshore facility where operation and maintenance have a relatively large contribution in the total energy production cost. Another advantage of the VAWTs is the fact that the generator can be placed at sea level, reducing the complexity of the installation and maintenance. Additionally this characteristic improves the stability of the structure and, moreover, it would reduce the dimension and cost of the base. The concerns about the size and weight of the generator are minimized, favoring the installation of heavy direct drive generators with permanent magnets [10]. All these features of VAWTs show higher potentials for scalability, taking into account the operational inconveniences in HAWTs produced by the yawing system and the generator location. Both European and North American research programs are studying the feasibility of floating large VAWT [11, 12].

VAWT operation is characterized by complex and unsteady three-dimensional fluid dynamics, which presents considerable challenges for both description through measurements and numerical modeling [13]. Moreover, VAWTs are inherently exposed to cyclic variation in the angle of attack, giving cyclic blade forces which can produce material fatigue damage. As the energy conversion process in VAWTs is based on the variation of the blade's circulation along its rotation, the produced wake differs significantly to the one created by HAWTs: the near wake structure is strongly dominated by the effects of the vortices produced on the blade tips (end effects) and the angle of attack variations, these create recovery levels because of the vertical flow transport which is larger than the one produced by the turbulent fluctuation [14]. This characteristic is not present in HAWTs.

As long as the interest for designing and analysis of VAWT facilities is increasing, there will remain a need for reliable numerical models to characterize the VAWTs flow dynamics, thereby correctly predicting the wake recovery and allowing for the precise evaluation of the most efficient turbine array layouts.

Several models have been tested for the prediction of the important three-dimensional effects in the VAWT wake. For example, fully-resolved body-fitted grid simulations using Reynolds-averaged Navier-Stokes (RANS) turbulence models have shown a satisfactory performance to characterize the average performance and near-wake structure of the VAWT. However, accuracy depends on the turbulence model [15–19]. Nevertheless, these geometrically fully-resolved models have large computational costs since they have to solve the governing equations in local highly refined grid regions close to the blade boundary layers. This fact restricts the implementation of the model for a solution in a large scale facility (wind farms, for example), due to its non-viable calculation time. Another approach is to simulate the blades by using the so-called actuator line technique, which is an unsteady method that uses an external force model to solve the loads on the blade elements location and apply them as a body force term into the momentum equation, hence, it excludes the need of solving the boundary layer flow. This fact dramatically reduces the computational expenses and makes it feasible to run studies of the wake of VAWT and VAWT wind farms [20–23].

The present work studies the resulting wake of an H-shaped VAWT using an actuator line model (ALM), identifying the most relevant aerodynamic phenomena involved. First, the mathematical description of the model is presented together with the description of the studied VAWT. Then, the obtained results are presented for the spatial and temporal sensitivity in order to evaluate the response of the model to the variation of the mesh and time discretization, and its influence on the accuracy of the results. Different turbulence models were tested for analyzing their performance, and therefore, to define the reliability of each one. Additionally, a study of the operational turbine without the struts and without the tower was carried out for quantifying the contribution of these turbine components on the general wake structure. Simulated velocity and vorticity fields of representative sections are used for the flow analysis and they were also compared against measurements from a VAWT performing in the Open Jet Facility (OJF) of the Delft University of Technology, obtaining a good agreement, and for which experimental activity and results are reported in [24]. All the obtained results from the different tests mentioned above can be used as a practical reference guideline for choosing parameters in VAWTs simulations using the ALM. The model presents stability and accuracy, which makes it a potential suitable tool in the design of VAWTs for the prediction of the wake structure.

2. METHODOLOGY

The blade force equations were solved using an ALM (a blade element method) coupled to a dynamic stall model (DSM) [25]; the former samples the flow velocity from the Navier-Stokes solver, and therefore calculates the angle of attack and relative velocity for each blade element. The DSM is used to calculate dynamic blade force coefficients, which the ALM uses to impart the body forces back into the flow solver as a body force term in the momentum equation. A large eddy simulation (LES) model was then used for predicting turbulence effects.

In the present study, the focus was on wake modeling rather than loading or power prediction. For this work, the *turbinesFoam* library, developed by Bachant et al. [26–28], was used for the implementation of the ALM using the OpenFOAM open-source CFD framework. In previous work, the model had been validated against wind tunnel data for force coefficients in a pitching blade, with reasonable agreement [25]. The employed ALM and DSM are described in detail in [27] and [29], respectively, and only a brief description is given here.

2.1. Actuator Line Model

Based on the classical blade element theory, the ALM is a three-dimensional and undsteady aerodynamic model developed by Sørensen and Shen [30], and it is used to study the flow around wind turbines. In the ALM, turbine blades are divided into n-blade elements that behave aerodynamically as two-dimensional airfoil profiles. The forces are determined through a dynamic stall model commonly based on empirical data. The original governing Navier-Stokes equations are filtered for using the LES approach, and based on an incompressible fluid case

$$\frac{\partial \tilde{u}_i}{\partial x_i} = 0 \tag{1}$$

$$\frac{\partial \tilde{u}_i}{\partial t} + \frac{\partial \tilde{u}_i \tilde{u}_j}{\partial x_j} = -\frac{1}{\rho}\frac{\partial \tilde{p}}{\partial x_i} + \nu \frac{\partial^2 \tilde{u}_i}{\partial x_j \partial x_j} - \frac{f_i}{\rho} - \frac{\partial \tau_{ij}}{\partial x_j} \tag{2}$$

where $\tilde{u}_i$ and $\tilde{p}$ correspond to the velocity and pressure grid-filtered values, respectively, ν is the kinematic viscosity, f_i the acting body (blade) forces and τ_{ij} is the sub-grid scale (SGS) stress defined as $\tau_{ij} = \widetilde{u_i u_j} - \tilde{u}_i \tilde{u}_j$.

The sectional drag and lift coefficients considered in this work are taken from the technical report of Sheldahl and Klimas [31], which is a well-known database containing the values for a wide range of Reynolds numbers, and these values are used as an input into the DSM. The coefficients are linearly interpolated from a table, per the local angle of attack, then combining with the blade element approach the body forces acting on the blades are determined. A diagram of a cross-sectional airfoil element at radius r in the plane perpendicular to the turbine axis is depicted in Fig. 1. The relative

flow velocity V_{rel} and the angle of attack α are obtained for each blade through the geometric relation between the blade velocity V_{blade} and the local incident flow velocity V_{in} which is commonly lower than the asymptotic velocity V_{∞}

$$\vec{V}_{\mathrm{rel}} = \vec{V}_{\mathrm{in}} - \vec{V}_{\mathrm{blade}} \tag{3}$$

It is common to consider the inflow velocity which is placed in the same location of the element. However, in the present work this is obtained through the averaged value from defined numbers of local velocity samples in the region around the element, which are symmetrically distributed. The blade velocity V_{blade} is Ωr, where Ω represents the angular velocity of the rotor and r the radius of the blade element.

To consider the dynamic stall phenomenon and its effect on the drag and lift curves, the Leishman-Beddoes DSM Model [32] with the modifications of Sheng et al. [33] and Dyachuk [29] was employed.

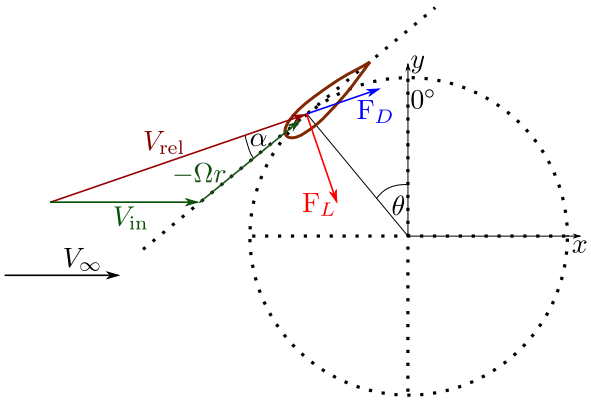

Figure 1. Illustration of velocity vectors and forces acting at the cross-section airfoil element

Once the angle of attack and relative velocity are obtained, the blade element lift and drag forces per length unit of spanwise are calculated as

$$f_L = \frac{1}{2}\,\rho\, c\, C_L\, |V_{\mathrm{rel}}|^2 \tag{4}$$

$$f_D = \frac{1}{2}\,\rho\, c\, C_D\, |V_{\mathrm{rel}}|^2 \tag{5}$$

where C_L and C_D are the lift and drag coefficients respectively. Both are function of the Reynolds number and the angle of attack. The lift force is orthogonal to the relative velocity $\vec{V}_{\mathrm{rel}}$ and the central axis, while the drag force is parallel to

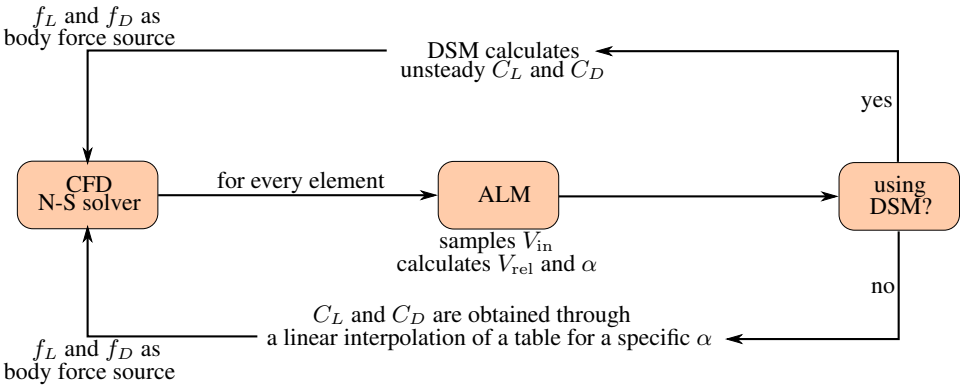

Figure 2. Flow chart of the ALM combined with the DSM for every time-step

the relative velocity $\vec{V}_{\text{rel}}$. The chord length is represented by c. An overview of the ALM implementation coupled with the DSM is illustrated in Figure 2

The same procedure is used to obtain the forces from the shaft and blade support arms of the turbine. Once all these forces are calculated for the actuator lines, they are added as a source of body force per unit of density (under the assumption of incompressibility) in the equation for the conservation of momentum (Equation 2).

2.1.1. Force distribution

The applied forces in the ALM must to be distributed smoothly on several mesh cells in order to avoid instability produced by high gradients. A three-dimensional Gaussian kernel is employed for this purpose projecting the source force terms around the element location. This gives a smoothing function η which is multiplied by the computed force on the element location and then imparted on a cell with a distance $|\vec{r}|$ from the actuator line element quarter chord position:

$$\eta = \frac{1}{\epsilon^3 \pi^{3/2}} \exp\left[-\left(\frac{|\vec{r}|}{\epsilon}\right)^2\right]$$

The smoothing width parameter ϵ is chosen by the maximum value from three different contributions related to: the 25% of the chrod length, the mesh size and the momentum thickness due to drag force, and it is expressed as:

$$\epsilon = \max\left[\frac{c}{4}, 4\sqrt[3]{V_{\text{cell}}}, \frac{cC_D}{2}\right]$$

Where V_{cell} is the cell volume.

2.2. Dynamic Stall Model

The DSM used is able to calculate the unsteady effects for the lift, pitching moment and drag, resulting in the physical description of the aerodynamics. The presented results in this work correspond for an operating turbine with a tip speed

ratio (TSR) of $\lambda = 4.5$. Thus, dynamic stall effects can be neglected while the DSM is implemented regardless of change in conditions. In previous work [25], the model has been tested in different stall conditions (low, medium and deep), showing good agreement with experimental data.

3. SIMULATION PARAMETERS: VALIDATION CASE

An H-shaped VAWT model was studied. Experimental studies for this have been performed in the Open Jet Facility (OJF) of Delft University of Technology, and it is available in [24]. Phase-locked measurements were acquired at the turbine mid span plane and 7 representative vertical planes in order to study the resulting wake. The turbine consists of two rotor blades extruded from a NACA0018 aluminum airfoil profile of 1 m of height (H), a rotor diameter (D) of 1 m and a chord length of 0.06 m (c) and it is operating under a free stream inlet velocity of 9.3 m/s ($\vec{V}_\infty$). The blades have a constant rotational speed (Ω) of 800 rpm within a local Reynolds numbers of Re $\sim 2.1 \times 10^5$. The attachment point is placed at a distance of $0.4c$ from the leading edge. Two aerodynamically profiled struts NACA0018, with a chord of 0.023 m, make the connection between the blades and the turbine tower and they are installed at a distance of 0.2 m from the blade tips. The domain consists on a $13.7D \times 6.6D \times 8.2D$ test section and an octagonal jet in the inlet with a cross-section of $2.85D \times 2.85D$ and a contraction ratio of 3:1 as it is depicted in Figures 3 and 5.

A Cartesian coordinate system has been used with the origin placed at the center of the turbine at the equatorial blade plane, such that the x-axis is pointing positively in the downwind direction. A positive angular rotation in counter-clockwise direction is seen from the top of the turbine.

Figure 3 shows the drawing of the used turbine and the schematic of the blade motion on a VAWT.

The whole turbine geometry has been considered in the numerical analysis including: blades, struts and the central shaft. The used domain of the study cases has the same geometry as the experimental campaign at the OJF [24]. No-slip velocity conditions were considered at the walls.

4. RESULTS AND DISCUSSION

In this section, obtained velocity and vorticity fields for representative sections are analyzed in order to study the evolution of the wake behind the operational VAWT. These results have been compared against the experimental data. A large eddy simulation (LES) model was used to predict the turbulence effects.

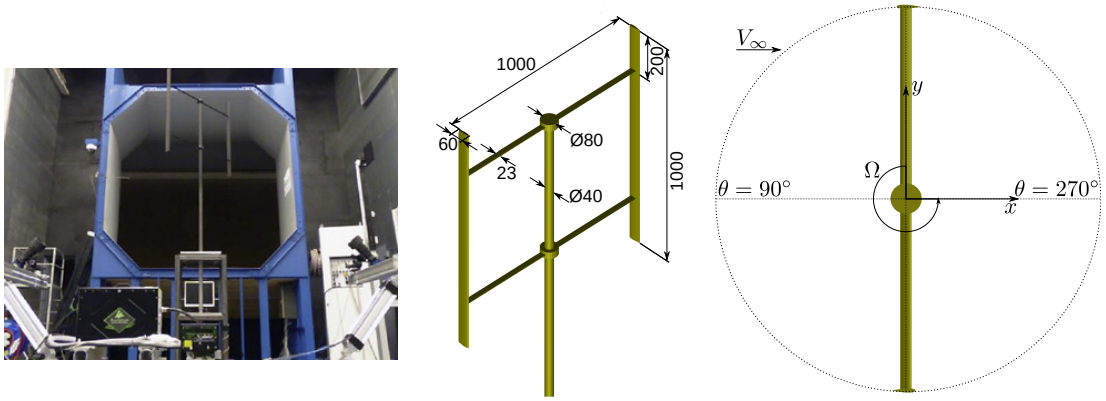

Figure 3. OJF tested turbine in [24] (left), 3D drawing of the simulated VAWT for this study with dimensions in [mm] (center) and schematic of the blade motion (right)

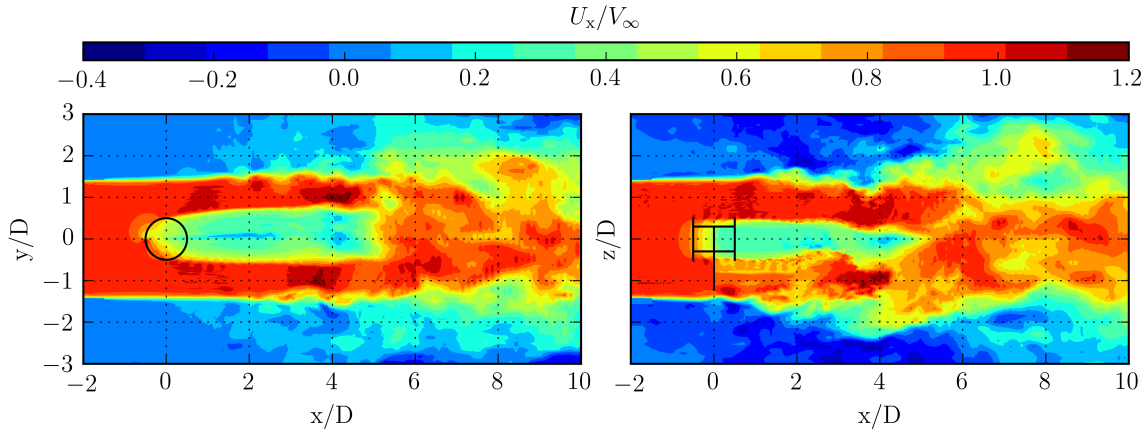

Figure 4. Instantaneous normalized streamwise velocity in the horizontal (left) and vertical (right) middle plane

Figure 4 depicts the obtained instantaneous streamwise velocity fields for the whole domain in the horizontal and vertical plane, respectively. The jet flow at the inlet and its expansion is clearly identified as well as the blockage produced by the operating turbine. The general structure of the wake is characterized by a vertical shrinking and a horizontal expansion as the flow moves downstream until it breaks to start the recovery process, the region where the wake breaks can be identified. The length of the chamber is not large enough to produce the full recovery of the wake. Stagnation (recirculation) areas are produced around the inlet jet.

4.1. Verification

4.1.1. Spatial sensitivity

A test of the response of the model to the variation in the mesh size has been carried out. Several domain discretizations were tested using different (maximum) mesh resolutions of D/40, D/80, D/96 and D/112 cells, corresponding to domains with 1.5×10^6, 8.39×10^6, 13.5×10^6 and 21.1×10^6 mesh cells, respectively. All the discretized domains have the same mesh topology: an uniform hexahedral distribution of cells with local refinement level of $n = 4$ (the cell of reference is divided equally in $2^{3n} = 4096$ sub-cells) in the region close to the rotor of the turbine and which is gradually surrounded by zones with lower refinements levels, in order to capture the wake details where it is produced. This topology was kept constant and globally refined: the mesh has been proportionally scaled in all the coordinates. The finest refinement region covers: $0.9D$ and $3.3D$ from the central shaft to the negative x-direction (upwind) and x-direction (downwind). It equally covers $0.9D$ from the origin in both horizontal y-directions perpendicular to the incoming flow and $0.8D$ from the equatorial blade section in both vertical z-directions. Figure 5 shows the whole computational domain with its dimensions and details of the employed mesh topology.

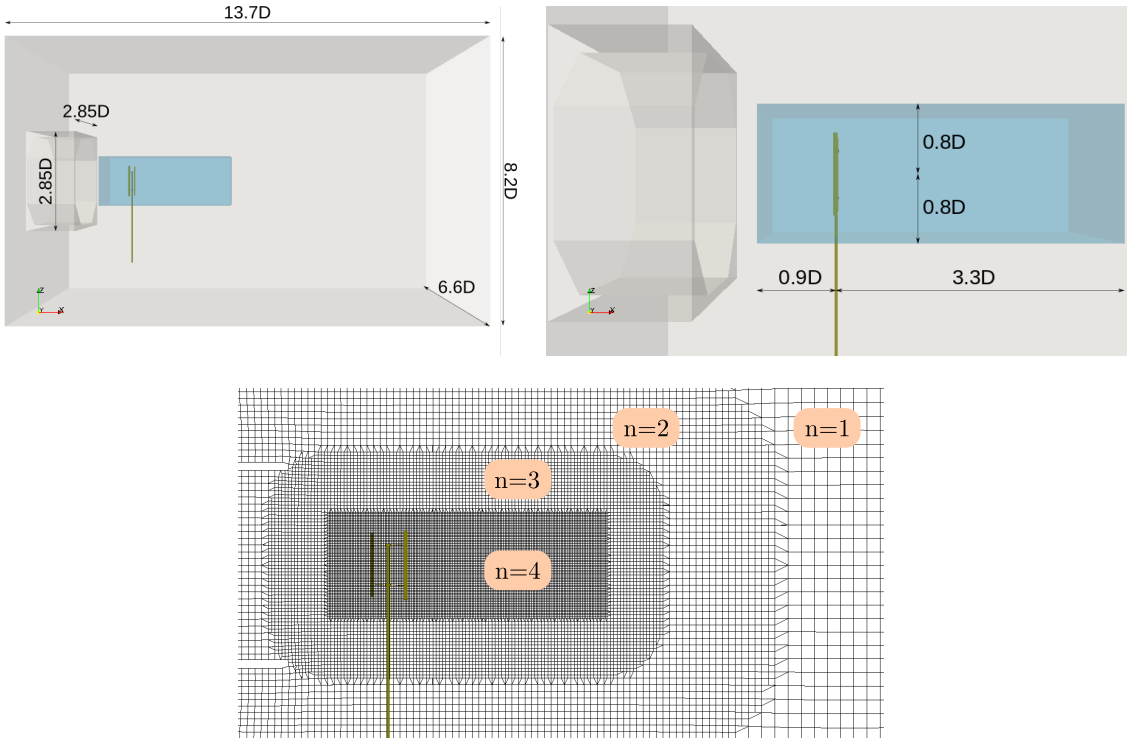

Figure 5. x-z view of the chamber domain, the operational VAWT turbine with the finest refinement region within the blue box (left), a detailed zoom at the entrance of the chamber (right) and a vertical section showing the different refinement levels of the mesh topology (bottom).

Figure 6 reveals the variation on the obtained results for the streamwise velocities varying the size of the mesh discretization for different sections of the domain. All curves have good agreement with the experimental results, there is not a considerable improvement in the accuracy by increasing the mesh resolution. However, it is observed that the curves are more irregular in shape when using a bigger mesh size because the model is able to capture more details from the wake with the finer discretization.

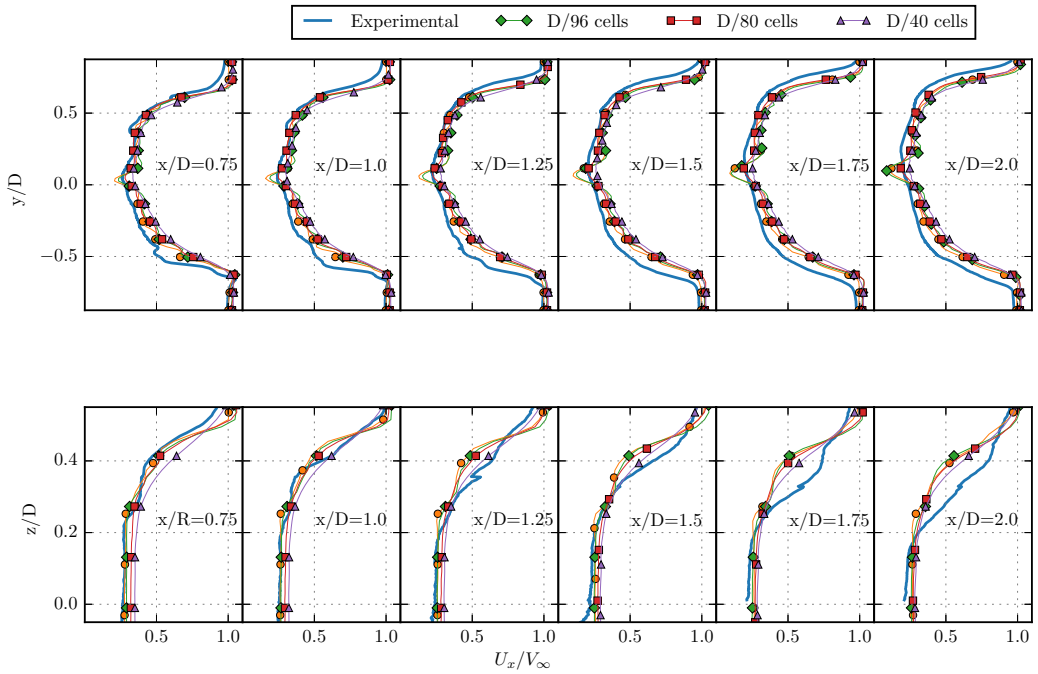

Figure 6. Comparison of the spanwise (top) and vertical (bottom) profiles of the normalized mean streamwise velocity at different downstream sections x/D, for domain meshes with D/80, D/96 and D/112 cells

Figure 7 shows the angle of attack and normal force response during one revolution for simulated values, varying the number of mesh points of the domain. There is a small difference in the results for the values of azimuthal angle close to 90°. There is an evident trend to a convergence with the increasing of the mesh resolution for the obtained results of the angle of attack.

Figure 8 depicts the vorticity field for two different discretized meshes. The larger mesh resolution produced better simulation of the vortices created by the blades, which are essential for identifying and representing the far wake recovery (in open sites, for example).

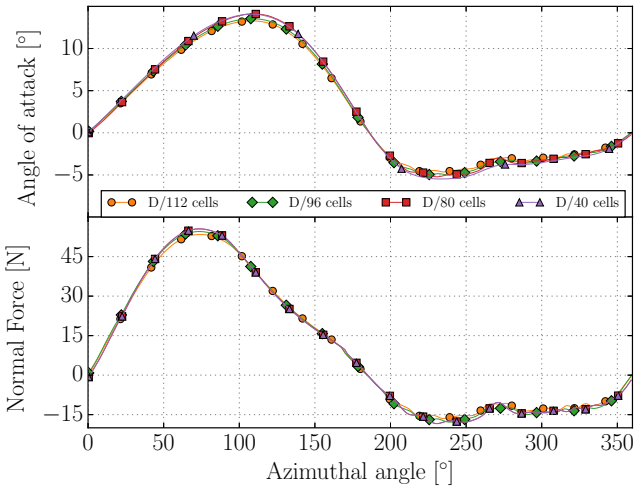

Figure 7. The angle of attack (top) and normal force (bottom) response for domain meshes with D/80, D/96 and D/112 cells

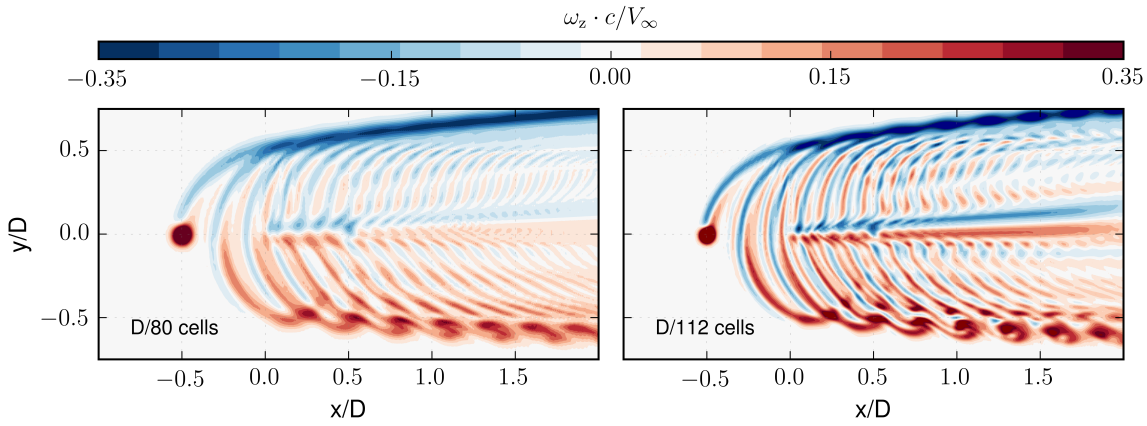

Figure 8. Contours of normalized out of plane vorticity for the horizontal plane using different discretization of the domain

4.1.2. Temporal sensitivity

Another concern for validating the model is the temporal sensitivity verification. Different maximum Courant numbers (Co) values were chosen for a varying temporal discretization test: $Co = 0.25$, 0.50 and 0.95. In this study a mesh with $D/80$ cells was used. The variation of the obtained angle of attack is evaluated for one revolution using the different Co. The maximum Courant number limit is given by Courant-Friedrichs-Lewy (CFL) condition, necessary for the convergence: its value should be lower than unity. On the other hand, small time-step discretization could carry numerical instabilities due to the fluctuation of the flow fields resolving the transient term $\frac{\partial}{\partial t}$. For the case using $Co = 0.25$ the time discretization is such that the blades do not move more than one grid cell per time-step in the mesh region with local refinement. When the streamwise velocity profiles from Figure 9 are compared with Figure 6, the results were more sensitive for varying

the mesh size than the time-step discretization. Previous works carried out by Bachant [27] and Mendoza [25] showed the same characteristic. There is no relevant difference on the obtained fields between the case with $Co = 0.25$ and 0.5, results start to differ for $Co = 0.95$, and therefore, the latter is not a recommended value to work with since it could affect the accuracy on the results.

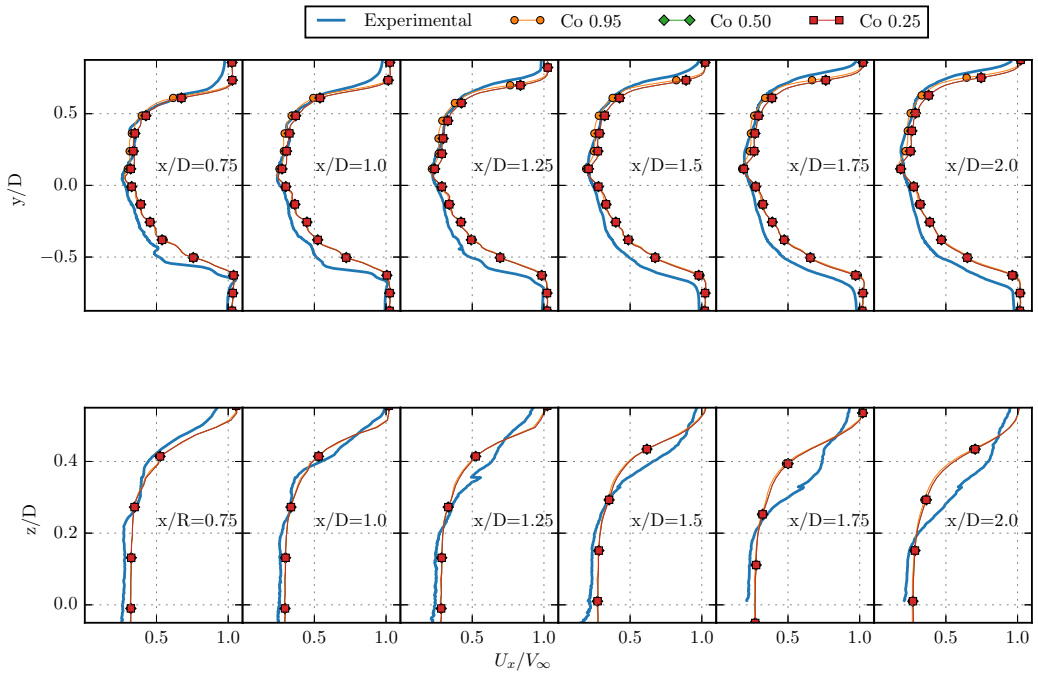

Figure 9. Comparison of the spanwise (top) and vertical (bottom) profiles of the normalized mean streamwise velocity at different downstream sections x/D, for maximum Courant numbers equal to 0.25, 0.5 and 0.95

Regarding the blade response during one revolution, Figure 10 reveals that there is a small change in the value of the angle of attack for the azimuthal angles close to 90°, which is the same behavior as was shown in the spatial sensitivity study (Figure 7). Nonetheless, the change is less sensitive for the temporal discretization test. In the second half of the revolution (between 180° and 360°), there is a more pronounced variation between the different results, specifically in the case using Co = 0.95. This can be produced by the influence of the change in temporal discretization over the resulting flow from the first half of the revolution within the rotor. These curves have been obtained using the values from the last revolution of the different cases.

4.1.3. Turbulence model comparison

Three different turbulence models have been tested in order to evaluate their performance and accuracy: Smagorinsky [34], dynamic k-equation [35] and dynamic Lagrangian [36]. In the latter model, the Smagorinsky constant C_s is

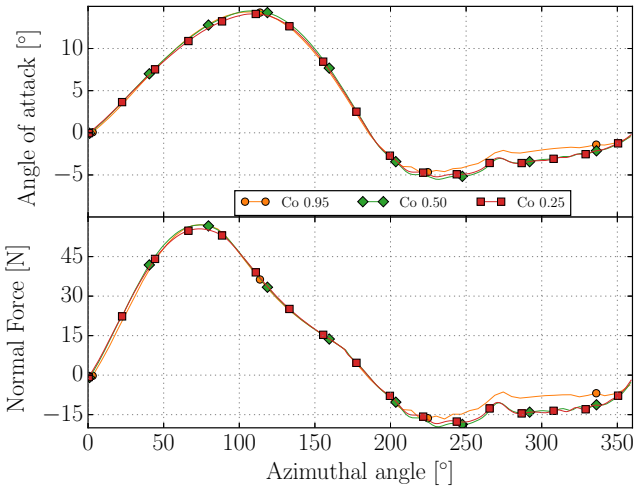

Figure 10. The angle of attack (top) and normal force (bottom) response for maximum Courant numbers equal to 0.25, 0.50 and 0.95

dynamically computed based on the information provided by the resolved scales of motion with a Lagrangian-concept averaging procedure, while in the standard Smagorinsky model, C_s is a chosen value which for this study is equal to 0.17.

The comparison of the obtained velocity profiles in Figure 11 shows a small difference between the individual models and good agreement with experiments for all of them.

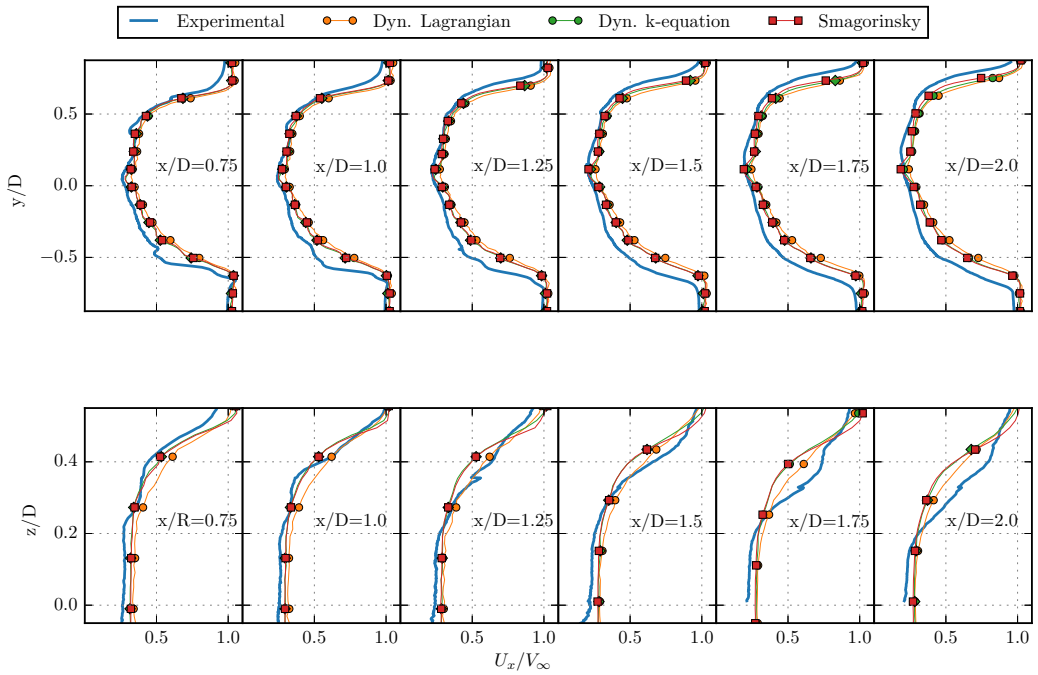

Figure 11. Comparison of the spanwise (top) and vertical (bottom) profiles of the normalized mean streamwise velocity at different downstream sections x/D, for Smagorinsky, dynamic k-equation and dynamic Lagrangian turbulence models

It is shown in Figure 11 that for the dynamic Lagrangian case, the results slightly differ from the other turbulence model. However, this variation is not relevant and it can not be considered either as an improvement or diminishment in terms of the accuracy.

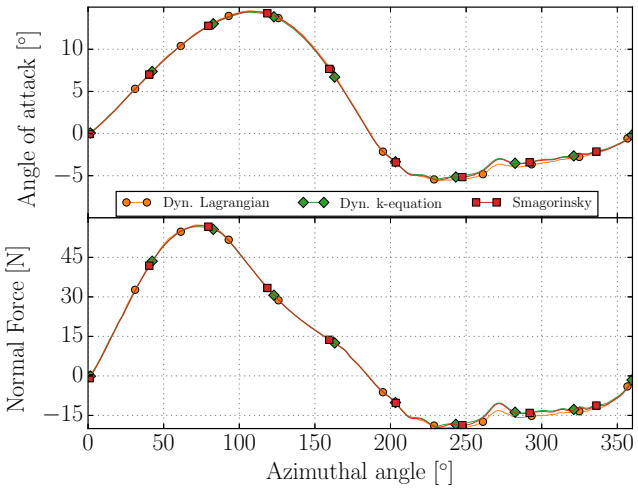

Figure 12. The angle of attack (top) and normal force (bottom) response for one revolution using different turbulence models

Figure 12 shows a similar pattern in the variation of the angle of attack and normal force using any of the models, there are no considerable differences. Therefore, the variation in the resulting velocity field (Figure 11) is dominated by the effect of the turbulence models and not by the force prediction.

Another group of essential quantities for characterizing the wake structure is the turbulence-related statistics. In Figure 13 the spanwise profile of the root-mean-square of absolute velocity is shown for different downstream locations. These profiles have two maxima in every studied section, which are located in the edges of the wake and are produced by the unsteady shed vorticity from the blades [37, 38]. Numerical results show a good representation of the profiles in terms of the trend. However, there is a lack in the representation of the fluctuations close to the center of the wake in the first studied sections ($x/D = 0.75, 1.0$ and 1.25). It can be considered that there is no one better model in terms of performance, since all of them have good accuracy with no distinguishably difference. Nevertheless, the dynamic k-equation and Lagrangian models performs better in the profile peaks with some overestimation of them in the further sections.

4.2. Model Validation

Once the response of the model for varying the mesh size, time discretization and turbulence approach have been tested, a series of simulations were carried out using the following configuration: a mesh with a resolution of $D/80$ cells for the spatial discretization, since it fulfills the LES turbulence and ALM domain resolution requirements. A maximum Courant

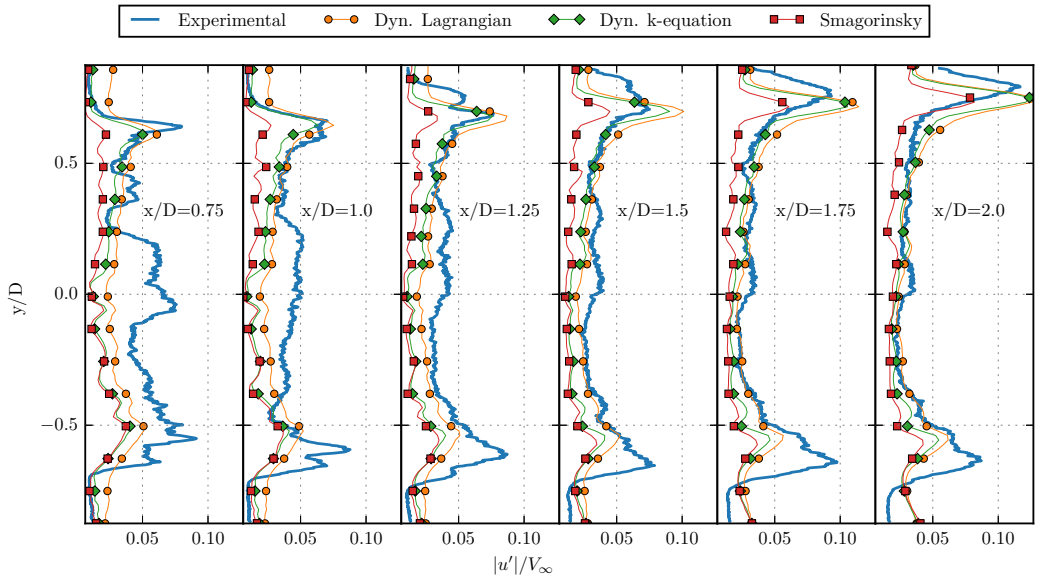

Figure 13. Comparison of the spanwise profiles of the normalized absolute velocity fluctuations at different downstream sections x/D, for Smagorinsky, dynamic k-equation and dynamic Lagrangian turbulence models

number of 0.25 in order that the blades move one cell per time-step. The LES Smagorinsky approach has been chosen for the turbulence effect prediction due to its low computational cost, and because this work focuses on the modeling part of the velocity field rather than the turbulence levels. The obtained results are presented in the following sections, and these are the average of phase-locked instantaneous velocity and vorticity fields.

4.2.1. Horizontal plane

Velocity and vorticity components are compared between numerical and experimental values. Figures 14, 15 and 16 depict the obtained fields for U_x, U_y and ω_z, which represent the streamwise velocity, cross-stream velocity and and out-of-plane vorticity components respectively. The plots of the experimental values are placed at the left and the simulated ones at the right side of the figures. The field values have been normalized using the asymptotic velocity and the chord length in order to facilitate the analysis and comparison. The lateral structure of the wake is identified and, therefore, the contribution from the blade pitch motion on it as well.

From Figures 14, 15 and 16 it can be noticed that there is a general good agreement for the wake prediction in the whole studied region, including the rotor region ($-0.5 \leq x/D \leq 0.5$). A pronounced wake is created by the rotating shaft of the turbine, and this wake is slightly inclined toward the y-direction. The simulated wake has a lower lateral expansion (in the y-axis direction) compared to the experimental one. This can be due to the lack of mesh resolution for reproducing

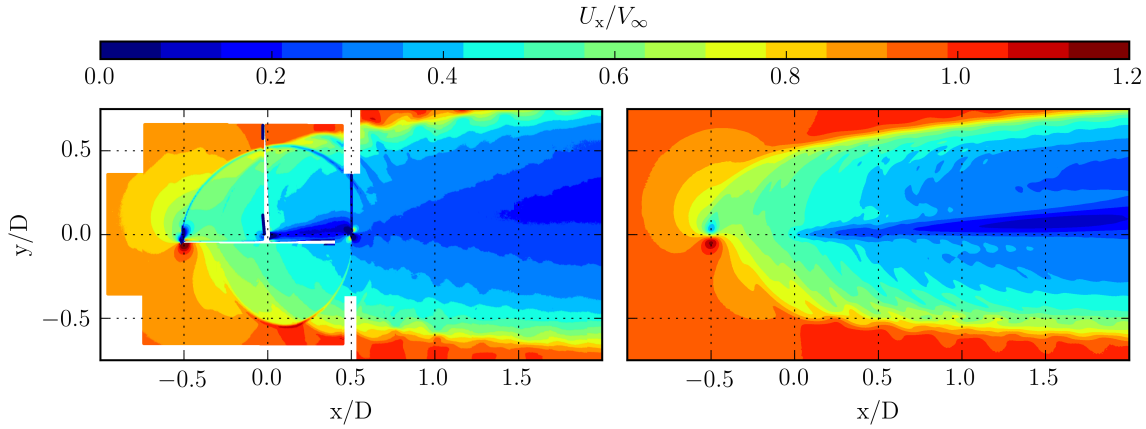

Figure 14. Normalized streamwise velocity in the horizontal middle plane for experimental (left) and numerical (right) results

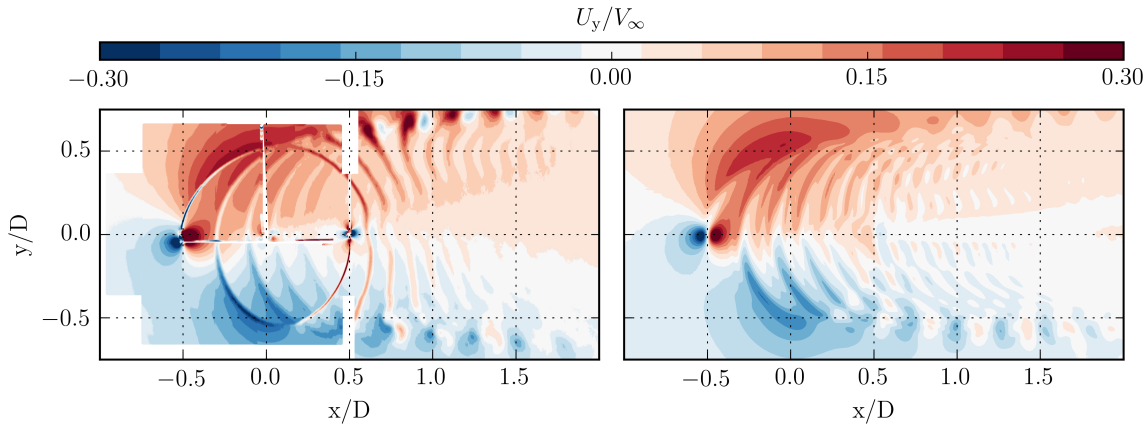

Figure 15. Normalized cross-stream velocity in the horizontal middle plane for experimental (left) and numerical (right) results

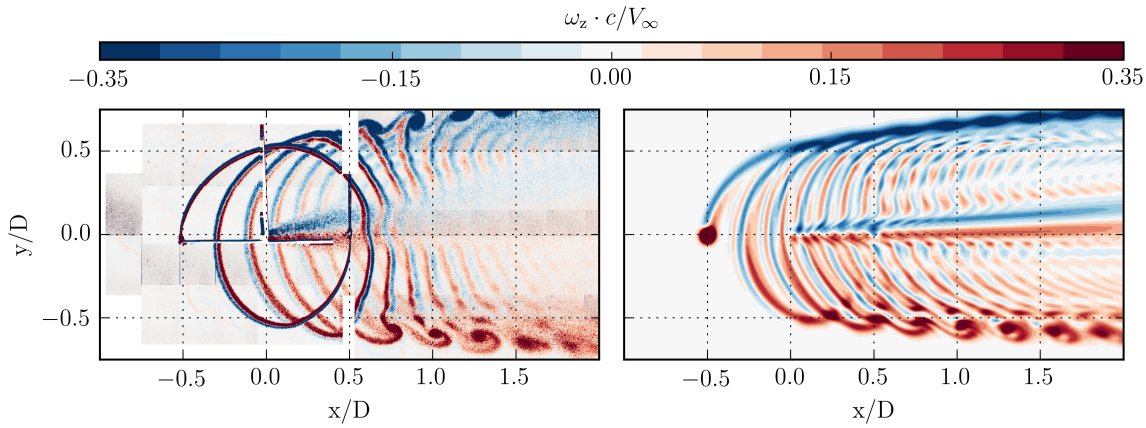

Figure 16. Normalized out-of-plane vorticity in the horizontal middle plane for experimental (left) and numerical (right) results

a proper shed vorticity from the blades. An asymmetric wake behavior is revealed in both experimental and simulated results with a larger region of velocity deficit in the y-direction. This can be produced by two different main contributions: vortex shedding and the lateral flow transportation [39]. First, stronger vortex shedding and therefore more severe flow separation is produced where the blades move in the opposite direction of the main flow ($y > 0$). Second, the wake flow is transported to the y-direction due to the lower pressure produced by the blade wake in this region and the strong angular momentum in the downstream side which drags the wake flows. Figure 15 shows the lateral velocity field characterized by a flow transportation more pronounced in the y-direction.

A smaller region of higher wake deficit ($U_x/V_\infty \leq 0.2$) is present in the simulated results. Further, the numerical streamwise velocities are larger than the experimental results in the outer region of the wake ($U_x/V_\infty = 1.1$). Vortical structures generated by blades are dissipated along the main flow direction. Vortices structures were well simulated in the downwind direction after the rotor with more accurate size and location in the negative y-direction region ($y/D \leq 0$). Experimental and numerical results showed a smoothly effect due to their averaging process [24]. A good representation of the inner rotor wake and its interaction with the blade was made by the simulation. There is a uniform flow pattern within the rotor region and this is disturbed by the blade motion path, and previously by the shaft.

It is shown in Figure 16 that the chosen kernel width ϵ is too big. Comparing experimental and numerical results, a smaller value would produce shed vortical structures that match better the experiments. However, running simulations with such a small ϵ is too expensive in terms of computational cost.

4.2.2. Vertical planes

Figures 17, 18 and 19 reveal the normalized streamwise, cross-stream and vertical velocity components respectively for different representative sections in the vertical plane ($y/D = -0.5, -0.4, -0.2, 0, 0.2, 0.4$ and 0.5), allowing us to represent and identify the vertical structure of the wake in terms of size, position and geometry, and also, the influence of the vorticity from the blade tips on it. As in the previous section, results are normalized using the asymptotic velocity and the chord length. In general, a good agreement with experimental values could be obtained in all the regions of every section. A better numerical representation can be noticed at the region close to the rotor and it loses concordance in the more distant areas. Vortical structures from the blade tips are well represented specially in the sections close to the vertical middle plane (y/D$\sim$0) and they are dissipated along the main flow direction (Figure 19). Their position is similar for both results but the size is underestimated in the numerical cases as it was for the horizontal plane, giving as a result a smaller expansion of the wake in both vertical and horizontal directions compared to the experimental data. Therefore, the simulated wake has a lower extension and intensity of the wake deficit. Pronounced effects by the shaft of the turbine on

the wake can be identified in the middle vertical plane ($y/D = 0$) for the streamwise velocity component, it is shown that the flow is strongly decelerated (color blue), starting at the location of the shaft $x/D = 0$.

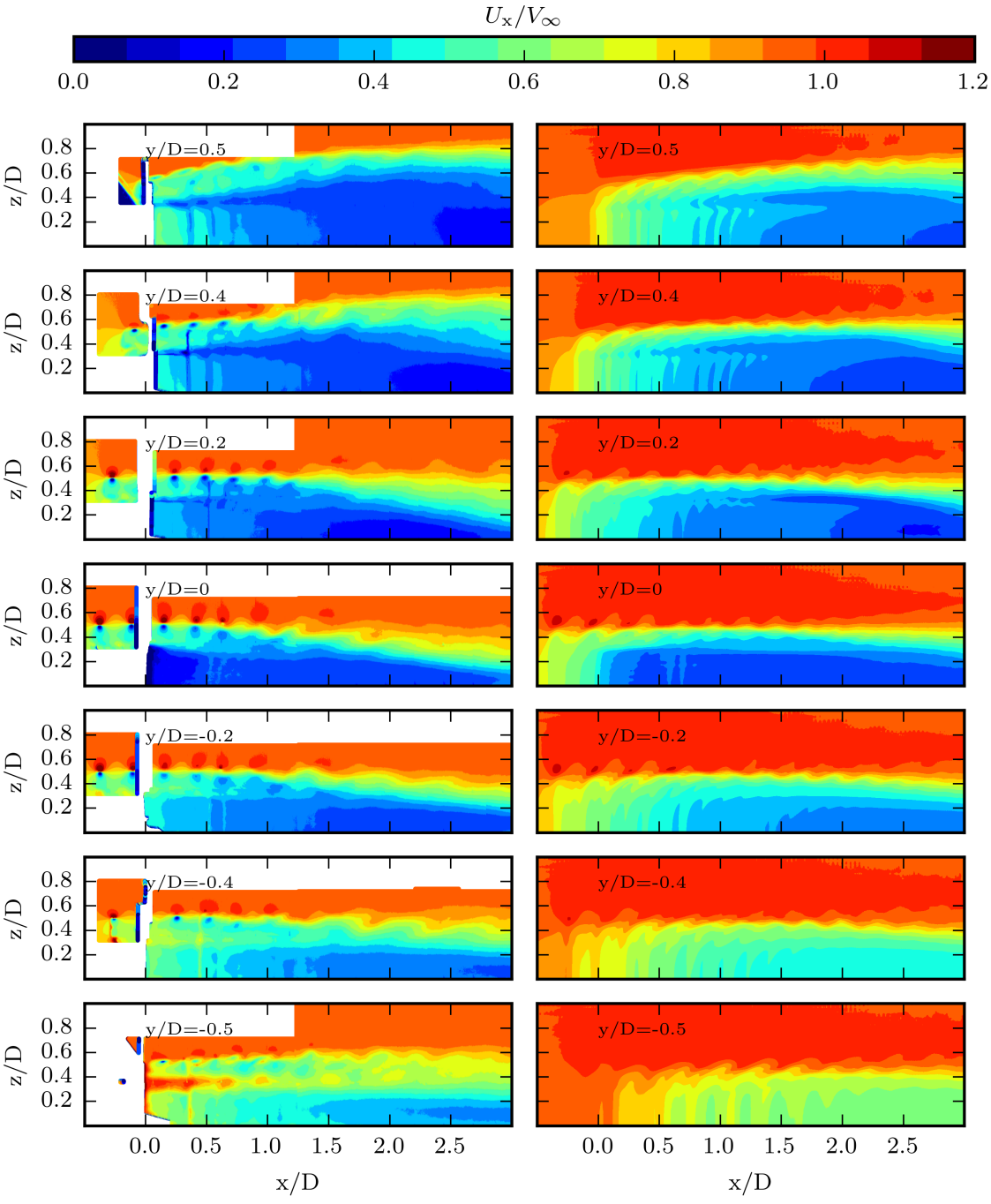

Figure 17. Normalized streamwise velocity at different representative sections in the vertical plane for experimental (left) and numerical (right) results

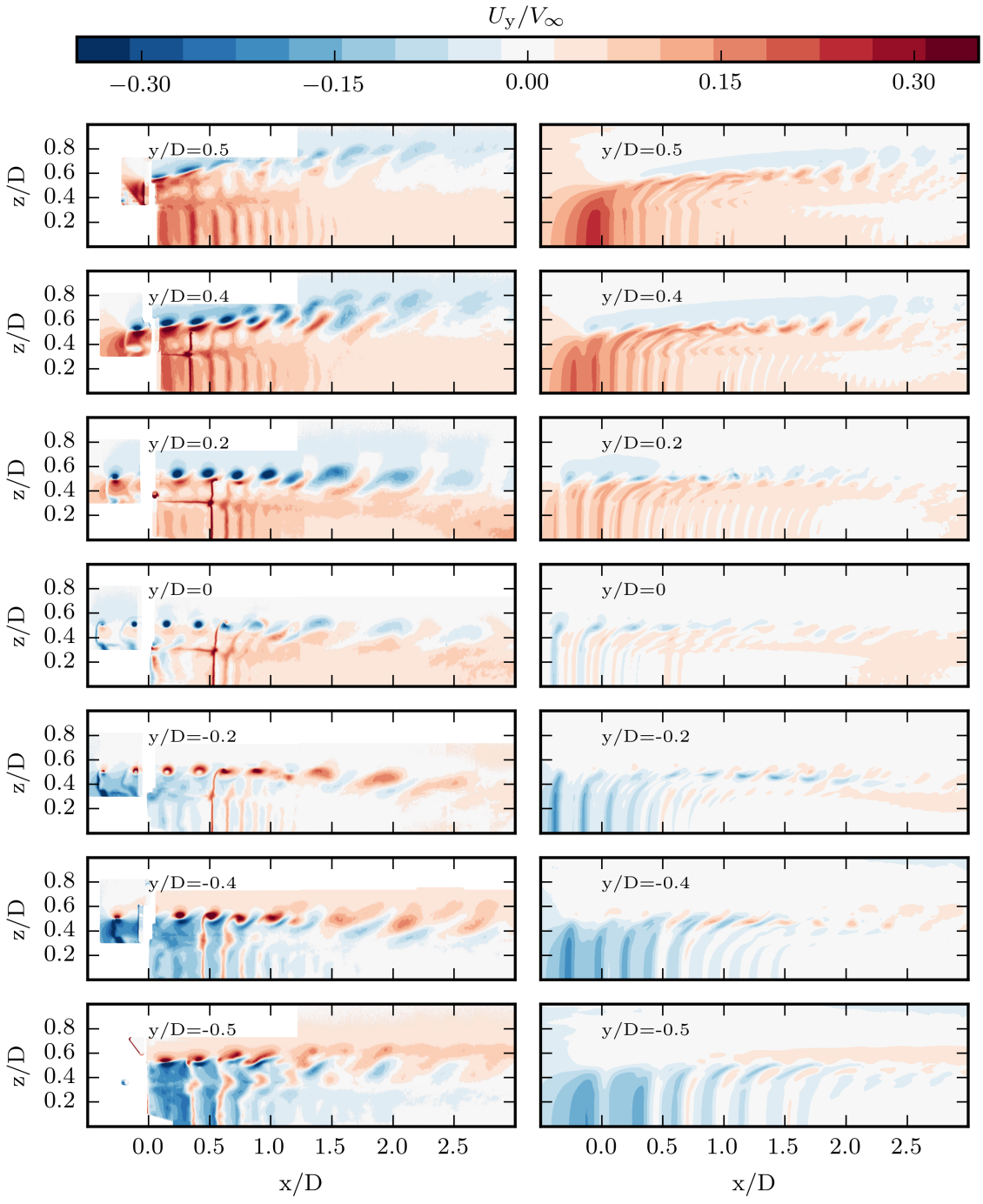

Figure 18. Normalized cross-stream velocity at different representative sections in the vertical plane for experimental (left) and numerical (right) results

Figures 18 and 19 are used for an inner wake analysis. The cross-stream flow shows the lateral expansion of the wake with the velocity components pointing outwards the middle plane: red colored areas in the positive y-direction and blue

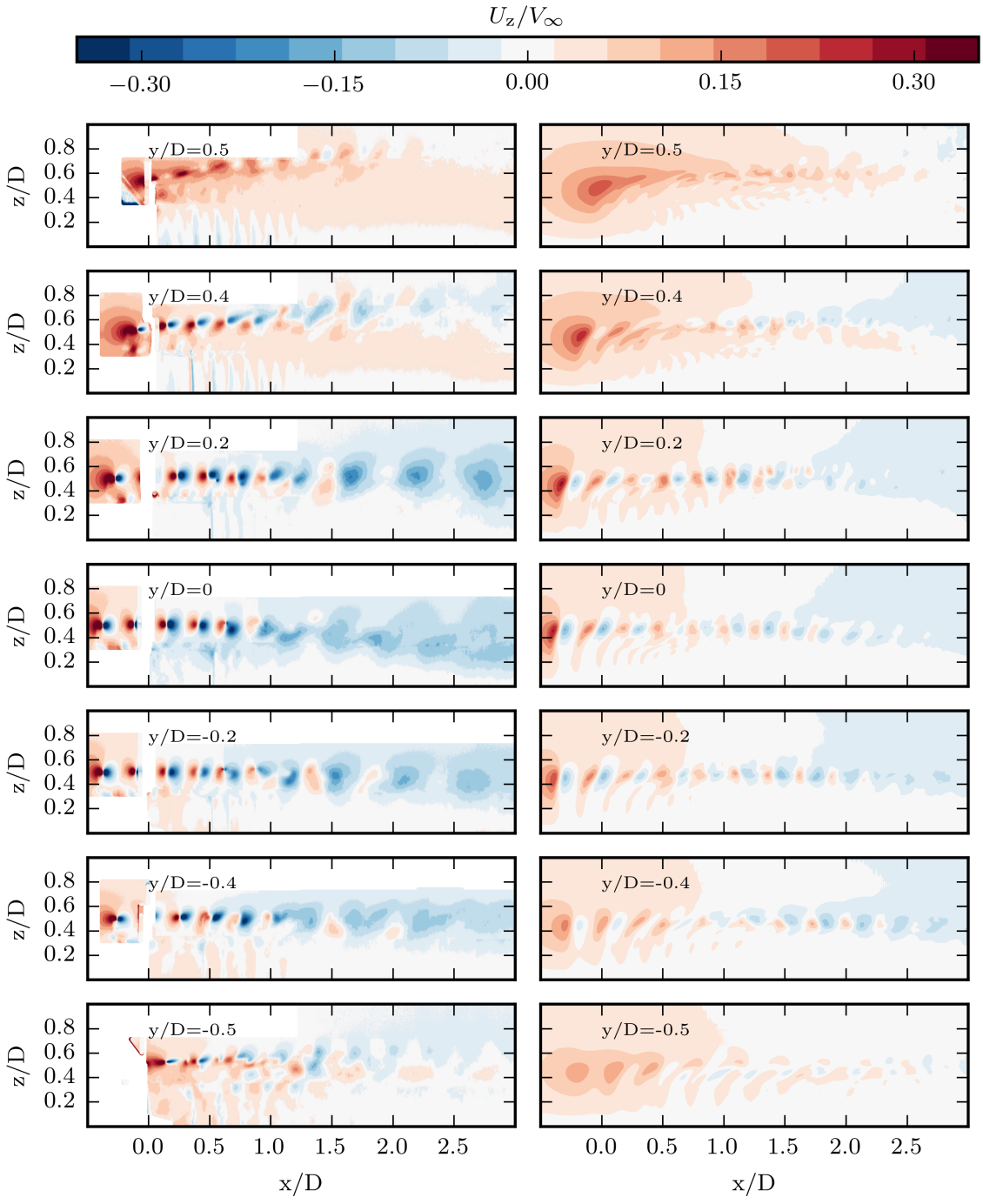

Figure 19. Normalized vertical velocity at different representative sections in the vertical plane for experimental (left) and numerical (right) results

colored areas in the negative y-direction. The cross-stream velocity has low values (close to zero) in the upper regions (z-direction) outside of the wake. The overall structure of the wake is well represented by the simulated values. However,

there are quantitative discrepancies, these are related to force prediction issues as was mentioned previously. The magnitude values of lateral and vertical velocities are more pronounced in the rotor region ($-0.5 \leq x/D \leq 0.5$) where the incoming flow faces the turbine and is blocked. From the vertical velocity plots it is noticed that numerical blade tips vortices have an inclination produced by the outer wake flow. On the other hand, experimental results show that the same vortices kept the vertical structure within the rotor region.

Figure 20 shows the cross-stream vorticity created by the turbine. The vortical structures produced by the two blade tips are similar in the position for both experimental and numerical results, but they differ in the shape. This can be inferred from their magnitude, propagation and dissipation within the flow. Vorticity produced in the struts position ($z/D = 0.3$) is also observed, but with lower intensity for experimental results. A pronounced vortical structure is generated by the tip of the tower which is clearly identified in the vertical middle plane ($y/D = 0$). A weaker blade tip vorticity representation was made by the simulation in the section $y/D = -0.5$. Again, as in the horizontal plane study, it is observed an oversized kernel width ϵ in the numerical results.

4.3. Additional tests

4.3.1. Struts and tower influence

A test of the influence of the struts and tower in the obtained fields was made. Three simulations were carried out: the complete turbine including all the components, removing only the struts and removing only the tower. Figure 21 depicts that the results have a good agreement with experimental values for all cases, which shows the main contribution for the wake structure is made by the blades.

The Figure 22 reveals the streamwise velocity component in different sections perpendicular to the main flow for the studied cases. The absence of the tower is easily identified in the region close to $y/D = 0$. A strong blockage is present where the blade moves in the opposite direction to the flow ($y/D \geq 0.5$) resulting in a wake expansion for this region, which increases in the downwind direction. The obstruction of the flow by the tower (central axis) is also captured and this keeps centered outside the wake. A considerable asymmetry was observed. The major blockage effect occurs in the cases with the complete turbine and removing the struts. In general, the blockage profiles have the same shape (geometry) with some variations within the wake, therefore the influence of the struts and tower are not relevant in the overall structure.

The normal forces in one blade for the different studied cases are revealed in Figure 23. In all cases, the major concentration of normal forces is located in the region between the struts and for the azimuthal position between $0^\circ$and 90°, when the blade faces directly in opposite direction to the incoming flow. For the case without considering the tower,

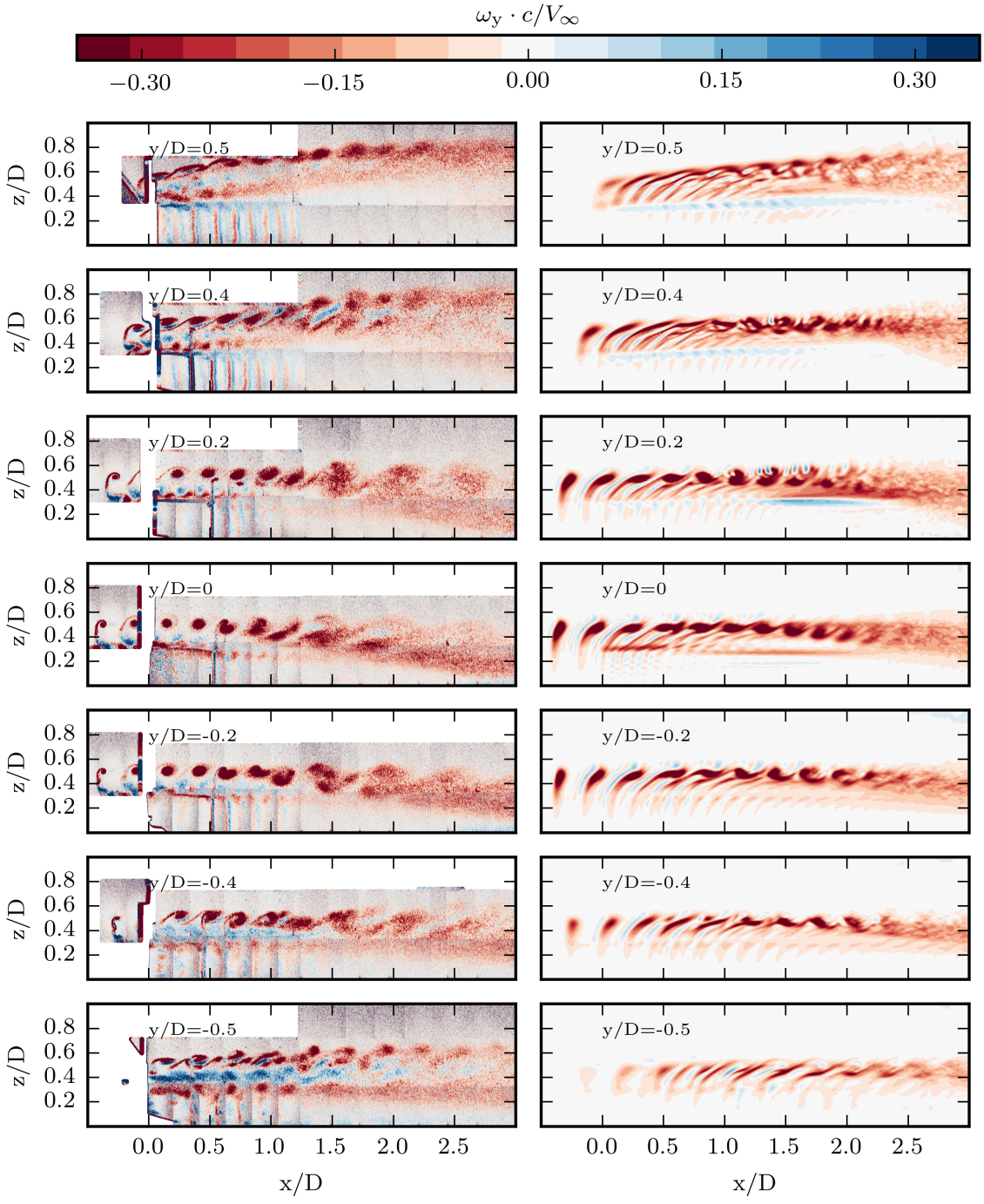

Figure 20. Normalized cross-stream vorticity at different representative sections in the vertical plane for experimental (left) and numerical (right) results

its absence is noticed in the azimuthal blade position around of 270° where there is no region with almost zero value of forces (white color) as in the other cases. There is not a proper representation of the strut-blade joint effects within the

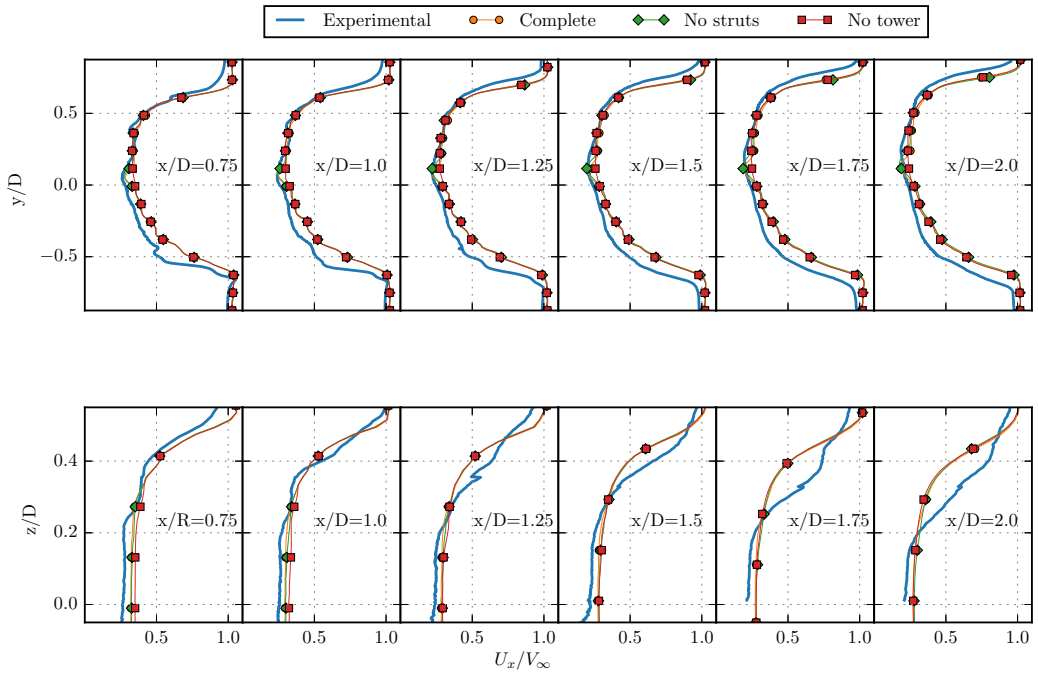

Figure 21. Comparison of the spanwise profiles of the normalized mean streamwise velocity at different downstream sections x/D, considering the complete turbine, without the struts and without the tower

results, since it is expected to have a reduction on the normal forces acting over the blades around (and between) the joints region.

Figure 24 reveals the influence of the tower in the streamwise velocity component. A lower blockage and the total lack of the wake produced by the tower are appreciable in it's absence. There is no relevant difference in the size and shape of the wake comparing the cases with and without tower.

4.3.2. Blade pitching sensitivity

The response to the variation in the pitching angle of the blades was looked at this study. The blades of the operating turbine were pitched 1° from the leading edge towards the inside of the rotor. The test was made using the coarser discretization of the domain. Figure 25 depicts the streamwise velocity profiles in representative sections. Due to the pitching, the resulting wake has a bigger lateral expansion in the y-direction, however these horizontal changes are not relevant in the general structure. Nevertheless, there is a relevant modification in the vertical wake structure, it has a more pronounced shrinking comparing to the test results without pitching blade. Therefore, the model is highly sensitive to the variation of the sampled angle of attack for the force prediction.

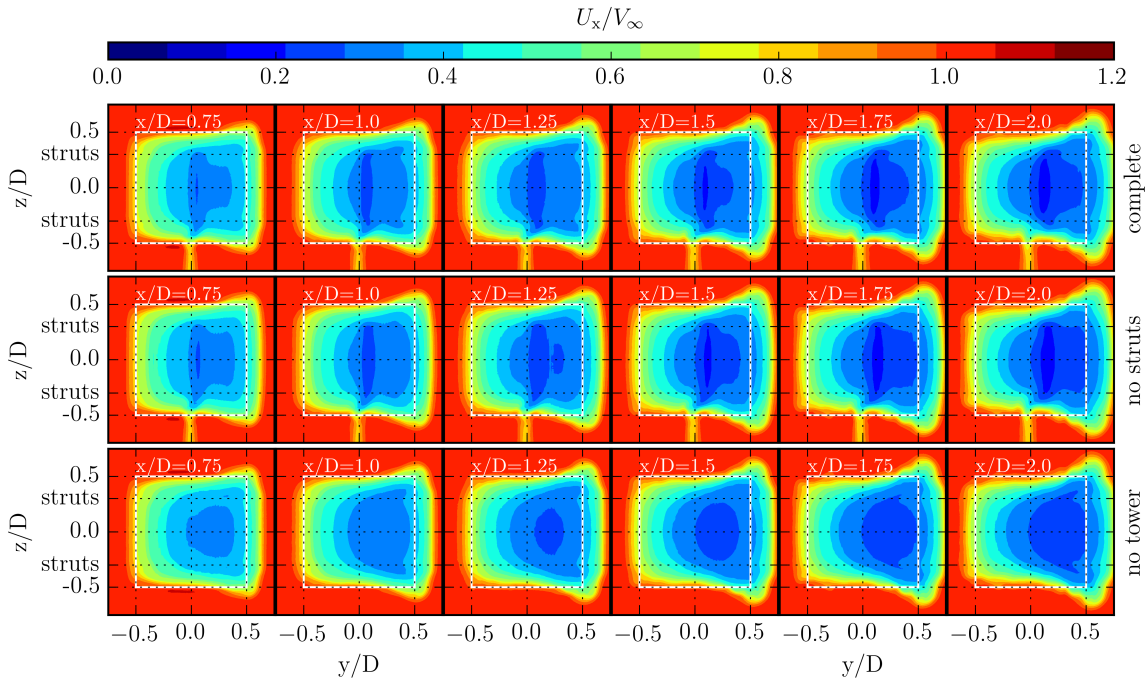

Figure 22. Normalized streamwise velocity at different representative sections perpendicular to the flow, considering the complete turbine (top), without the struts (center) and without the tower (bottom)

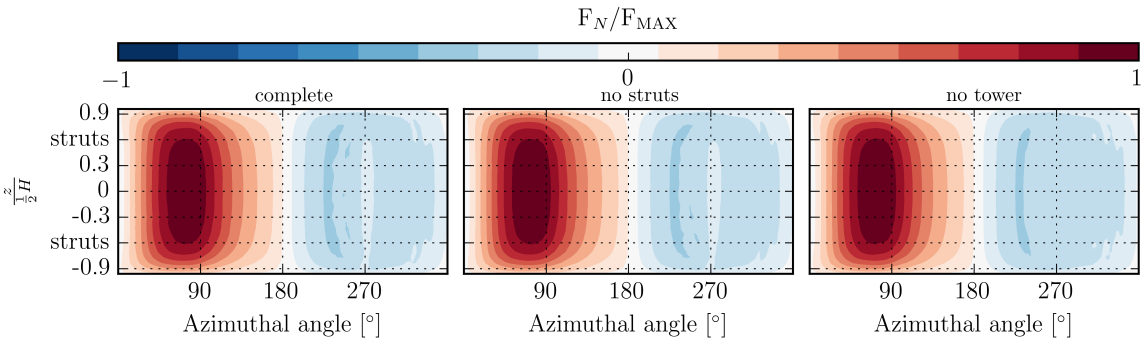

Figure 23. 3D normalized normal force distribution over the blade considering the complete turbine (left), without the struts (center) and without the tower (right)

4.4. General discussion

The results of 3D simulations presented herein show good agreement with experimental results.. However, the ALM is a simplified model which can represents the overall structure of the wake but there are some underestimation in the proper representation of the vorticity created by the blade tips and the struts, resulting in a less accurate simulated vertical wake expansion. The authors presume this could be caused by the high sensitivity that the model shows for the force prediction.

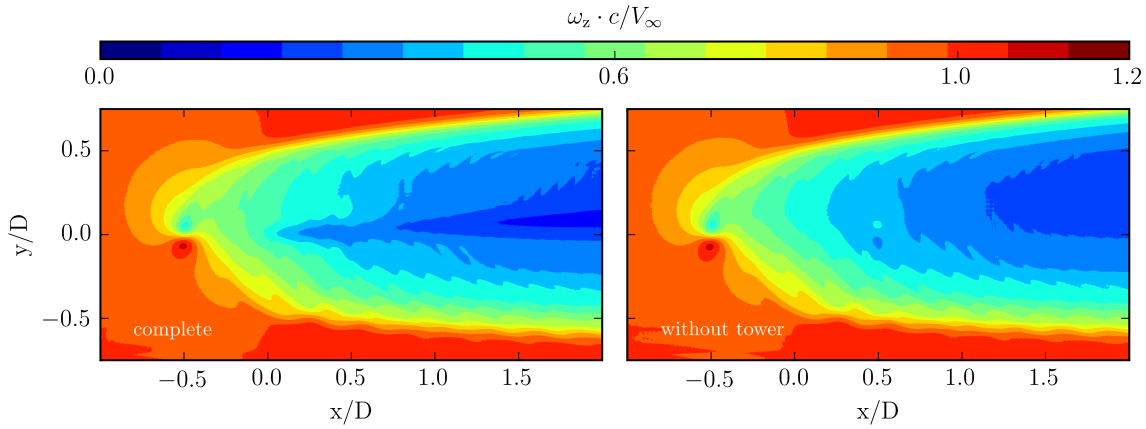

Figure 24. Normalized streamwise velocity in the horizontal middle plane for numerical results with (left) and without (right) considering the tower

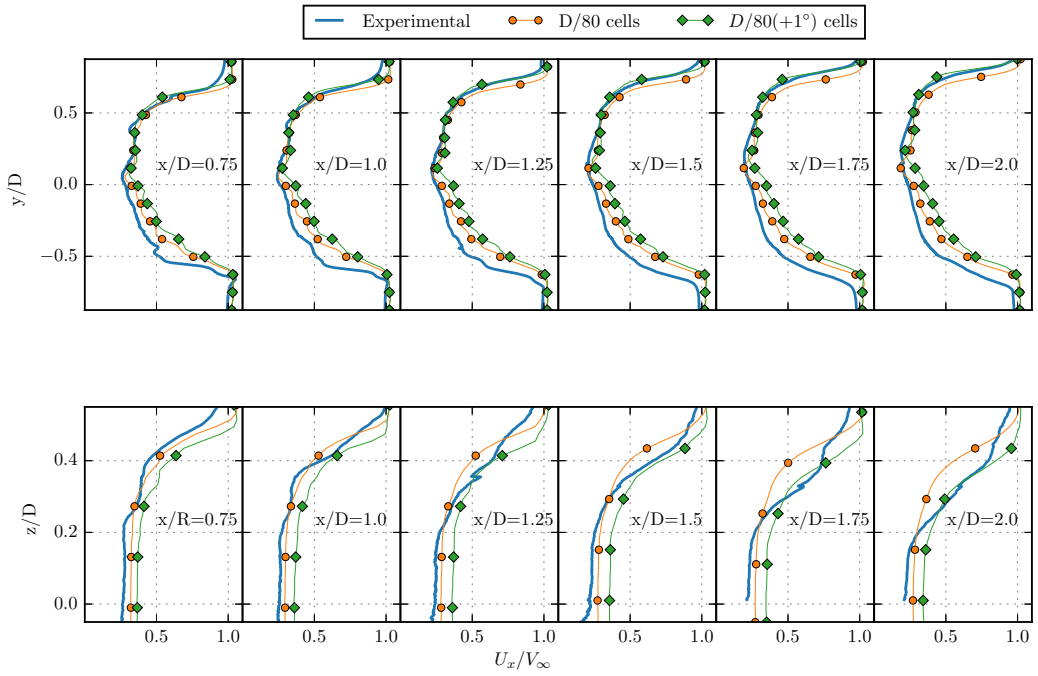

Figure 25. Comparison of the spanwise profiles of the normalized mean streamwise velocity at different downstream sections x/D, for a domain mesh with D/80 cells without blade pitching (left) and with a blade pitching of 1° (right).

In general, a numerical underestimation of the flow blockage by the rotor allowed the incoming flow to dissipate earlier the resulting operation turbine effects.

Considering all the presented results, there is a better model performance in the horizontal representation of the wake in the negative y-direction zone. The flow within the rotor has been properly reproduced by the model, capturing the flow

blockage produced by the tower and blade motion. Regarding the resulting velocity field, there is no sign of wake recovery until the further studied sections ($x/D = 2$), since the velocity deficit was still considerable. In terms of the blade force distribution, the joint of the struts with the blades was not considered by the model, therefore an improvement on the model force predictions is needed.

A proper prediction of the angle of attack is essential for a proper model performance. It has been shown that a variation in one degree of the pitch angle can produce a significant difference on the obtained results, moreover, the model is not that sensitive to the variation on the mesh size, temporal discretization or turbulence model. Therefore, all the parameters that are related to the angle prediction must be correctly implemented (as the flow curvature effects, blade attachment point, flow velocity sampling, etc).

It should be highlighted that one of the main advantage of the presented model may be the relatively low computational cost compared to a similar work carried out with a 3D full body resolved model.

5. CONCLUSIONS

A 3D actuator line model was used to simulate the resulting near wake of an operational VAWT, capturing the most relevant phenomena. This included the main characteristics of the flow pattern such as the horizontal expansion and vertical shrinking of the wake, velocity deficit regions (flow deceleration), inner-wake interaction with the blades, vortical structures creation from blade pitching and tips, etc.

The model was validated against measurements from an operational H-shaped VAWT, for which experimental activity has been performed at the Open Jet Facility (OJF) of TU Delft, showing good qualitative and quantitative agreement in general.

The model was tested in terms of the spatial and temporal sensitivity. Even using coarse meshes for the discretization of the domain did give accurate results, the details of the flow of the vortical structures however, were not accounted for. The results were not significantly influenced by changing the temporal discretization.

Three different turbulence models were used showing similar performance. It could not be claimed which one was the best for the simulations. For all the studied cases, the model did not show instabilities issues in the whole domain. The main structure of the resulting wake was not significantly affected by removing either the tower or the struts, which verifies that these parts do not contribute.

All the results obtained from the tested cases show the potential of the applied ALM for VAWTs simulations, which can then be used a reference practice guideline for choosing the propers parameters. The model showed numerical stability, which makes it a suitable for application in VAWTs simulations.

ACKNOWLEDGEMENT

This work was conducted within the STandUP for Energy strategic research framework and is part of STandUP for Wind. The computational works were performed on resources provided by the Swedish National Infrastructure for Computing (SNIC) at NSC.

REFERENCES

1. Paulsen US, Pedersen TF, Madsen HA, Enevoldsen K, Nielsen PH, Hattel JH, Zanne L, Battisti L, Brighenti A, Lacaze M, Lim V, et al. Deepwind-an innovative wind turbine concept for offshore. *EWEA Annual Event 2011*, 2011.
2. Sandia National Laboratories. Offshore use of vertical-axis wind turbines gets closer look. https://share-ng.sandia.gov/news/resources/news_releases/vawts/#.WKB9WHUrKp0. Accessed: 2017-02-12.
3. Dodd J. First 2MW vertiwind vertical-axis prototype built. http://www.windpowermonthly.com/article/1305428/first-2mw-vertiwind-vertical-axis-prototype-built. Accessed: 2017-02-12.
4. Borg M, Collu M, and Brennan FP. Offshore floating vertical axis wind turbines: advantages, disadvantages, and dynamics modelling state of the art. In *The International Conference on Marine & Offshore Renewable Energy (MORE 2012)*, pages 26–27, 2012.
5. Musgrove PJ. Wind energy conversion: recent progress and future prospects. *Solar & wind technology*, 4(1):37–49, 1987.
6. Steven Peace. Another approach to wind: vertical-axis turbines may avoid the limitations of today's standard propeller-like machines. *Mechanical Engineering-CIME*, 126(6):28–32, 2004.
7. Johan Ribrant and Lina Bertling. Survey of failures in wind power systems with focus on swedish wind power plants during 1997-2005. In *Power Engineering Society General Meeting, 2007. IEEE*, pages 1–8. IEEE, 2007.
8. Tavner PJ, Xiang J, and Spinato F. Reliability analysis for wind turbines. *Wind Energy*, 10(1):1–18, 2007.

9. Arabian-Hoseynabadi H, Hashem Oraee, and Tavner PJ. Failure modes and effects analysis (fmea) for wind turbines. *International Journal of Electrical Power & Energy Systems*, 32(7):817–824, 2010.

10. Sandra Eriksson, Andreas Solum, Mats Leijon, and Hans Bernhoff. Simulations and experiments on a 12kW direct driven pm synchronous generator for wind power. *Renewable Energy*, 33(4):674–681, 2008.

11. Sutherland HJ, Berg DE, and Ashwill TD. A retrospective of vawt technology. *Sandia Report No. SAND2012-0304*, 2012.

12. Vita L, Paulsen US, Pedersen TF, Madsen HA, and Rasmussen F. Deep wind: A novel floating wind turbine concept. *Windtech International*, 6(4):29–31, 2010.

13. Stephen A Huyer, David Simms, and Michael C Robinson. Unsteady aerodynamics associated with a horizontal-axis wind turbine. *AIAA journal*, 34(7):1410–1419, 1996.

14. Peter Bachant and Martin Wosnik. Characterising the near-wake of a cross-flow turbine. *Journal of Turbulence*, 16(4):392–410, 2015.

15. Peter Bachant and Martin Wosnik. Modeling the near-wake of a vertical-axis cross-flow turbine with 2-D and 3-D rans. *Journal of Renewable and Sustainable Energy*, 8(5):053311, 2016.

16. HF Lam and HY Peng. Study of wake characteristics of a vertical axis wind turbine by two-and three-dimensional computational fluid dynamics simulations. *Renewable Energy*, 90:386–398, 2016.

17. Andrea Alaimo, Antonio Esposito, Antonio Messineo, Calogero Orlando, and Davide Tumino. 3d cfd analysis of a vertical axis wind turbine. *Energies*, 8(4):3013–3033, 2015.

18. M Boudreau and G Dumas. Wake analysis of various hydrokinetic turbine technologies through numerical simulations. *Proceedings of AERO*, 2015, 2015.

19. Philip Marsh, Dev Ranmuthugala, Irene Penesis, and Giles Thomas. Three-dimensional numerical simulations of straight-bladed vertical axis tidal turbines investigating power output, torque ripple and mounting forces. *Renewable Energy*, 83:67–77, 2015.

20. Sina Shamsoddin and Fernando Porté-Agel. A large-eddy simulation study of vertical axis wind turbine wakes in the atmospheric boundary layer. *Energies*, 9(5):366, 2016.

21. Mahdi Abkar and John O Dabiri. Self-similarity and flow characteristics of vertical-axis wind turbine wakes: an les study. *Journal of Turbulence*, 18(4):373–389, 2017.

22. Sina Shamsoddin and Fernando Porté-Agel. Large eddy simulation of vertical axis wind turbine wakes. *Energies*, 7(2):890–912, 2014.

23. Victor Mendoza and Anders Goude. Wake flow simulation of a vertical axis wind turbine under the influence of wind shear. *Journal of Physics: Conference Series*, 854(1):012031, 2017.

24. G Tescione, D Ragni, C He, CJ Simão Ferreira, and GJW Van Bussel. Near wake flow analysis of a vertical axis wind turbine by stereoscopic particle image velocimetry. *Renewable Energy*, 70:47–61, 2014.

25. Victor Mendoza, Peter Bachant, Martin Wosnik, and Anders Goude. Validation of an actuator line model coupled to a dynamic stall model for pitching motions characteristic to vertical axis turbines. In *Journal of Physics: Conference Series*, volume 753, page 022043. IOP Publishing, 2016.

26. Peter Bachant and Martin Wosnik. Simulating wind and marine hydrokinetic turbines with actuator lines in rans and les. In *APS Meeting Abstracts*, 2015.

27. Peter Bachant, Anders Goude, and Martin Wosnik. Actuator line modeling of vertical-axis turbines. *arXiv preprint arXiv:1605.01449*, 2016.

28. Pete Bachant, Anders Goude, and Martin Wosnik. turbinesfoam: v0.0.7, April 2016. doi:/10.5281/zenodo.49422. URL http://dx.doi.org/10.5281/zenodo.49422.

29. Eduard Dyachuk. *Aerodynamics of vertical axis wind turbines: Development of simulation tools and experiments*. PhD thesis, Acta Universitatis Upsaliensis, 2015.

30. Jens Nørkær Sørensen and Wen Zhong Shen. Computation of wind turbine wakes using combined navier-stokes/actuator-line methodology. In *European Wind Energy Conference EWEC 99*, 1999.

31. Robert E Sheldahl and Paul C Klimas. Aerodynamic characteristics of seven symmetrical airfoil sections through 180-degree angle of attack for use in aerodynamic analysis of vertical axis wind turbines. Technical report, Sandia National Labs., Albuquerque, NM (USA), 1981.

32. JG Leishman and TS Beddoes. A generalised model for airfoil unsteady aerodynamic behaviour and dynamic stall using the indicial method. In *Proceedings of the 42nd Annual forum of the American Helicopter Society*, pages 243–265. Washington DC, 1986.

33. Wanan Sheng, RA Galbraith, and FN Coton. A modified dynamic stall model for low mach numbers. *Journal of Solar Energy Engineering*, 130(3):031013, 2008.

34. Joseph Smagorinsky. General circulation experiments with the primitive equations: I. the basic experiment. *Monthly weather review*, 91(3):99–164, 1963.

35. Won-Wook Kim and Suresh Menon. A new dynamic one-equation subgrid-scale model for large eddy simulations. In *33rd Aerospace Sciences Meeting and Exhibit*, page 356.

36. Charles Meneveau, Thomas S Lund, and William H Cabot. A lagrangian dynamic subgrid-scale model of turbulence. *Journal of Fluid Mechanics*, 319:353–385, 1996.

37. L Battisti, L Zanne, S DellAnna, V Dossena, G Persico, and B Paradiso. Aerodynamic measurements on a vertical axis wind turbine in a large scale wind tunnel. *Journal of energy resources technology*, 133(3):031201, 2011.

38. G Brochier, P Fraunie, C Beguier, and I Paraschivoiu. Water channel experiments of dynamic stall on darrieus wind turbine blades. *Journal of Propulsion and Power*, 2(5):445–449, 1986.

39. HY Peng, HF Lam, and CF Lee. Investigation into the wake aerodynamics of a five-straight-bladed vertical axis wind turbine by wind tunnel tests. *Journal of Wind Engineering and Industrial Aerodynamics*, 155:23–35, 2016.